Computational Study of the Structural, Mechanical and Optoelectronic Properties of Metal-halide Perovskites for Hybrid Energy Storage Applications

Batool AMINA [1], Gul NAZ [1], Nadeem MAJID [1], Ghulam Nabi AZEEM [2], Riaz Khalid NADEEM [3], Muhammad Arshad JAVID [1] *

[1] *Institute of Physics, Baghdad-ul-Jadeed Campus, The Islamia University of Bahawalpur, Bahawalpur, 63100, Pakistan*
[2] *Department of Physics, Hafiz Hayat Campus, University of Gujrat, Gujrat, 50700, Pakistan*
[3] *Department of Physics, University of Okara, Okara, Multan Road Renala Khurd Bypass, 56300, Pakistan*

http://doi.org/10.5755/j02.ms.42288

Received 21 July 2025; accepted 30 September 2025

Metal-halide perovskites (MHPs) are investigated in industrial applications due to optoelectronics and energy storage properties. In this study, the effects of hydrostatic pressure on the structural, electronic, elastic and optical properties of $CsPbM_3$ (M = F, Cl, Br, and I) are studied through using theoretical calculations based on the FP-LAPW method in Materials Studio, with GGA-PBE and LDA-CAPZ parameterizations. The exchange-correlation energies are calculated with GGA-PBE and LDA-CAPZ parameterizations. Results indicate that $CsPbCl_3$ with GGA-PBE exhibits the highest mechanical stability with a bulk modulus of 24.67 GPa, B/G ratio of 2.49, and positive elastic constants. $CsPbF_3$ (LDA-CAPZ) is the hardest (9.73 GPa) but mechanically unstable under pressure. Moreover, the $CsPbM_3$ exhibits a vertical-electron transition as well as semiconductor with a direct band gap at R- symmetry point as the band gap decreases between $CsPbF_3$ (2.629 eV PBE, 2.498 eV LDA) to CsPbI 3 (1.303 eV PBE, 1.280 eV LDA) respectively. A red shift in absorption and higher static dielectric constant occurs with increasing halide atomic radius. $CsPbI_3$ shows strong infrared and visible absorption, ideal for solar cells, while $CsPbCl_3$ and $CsPbBr_3$ keeps high plasmonic activity and suitable for high-frequency optoelectronic applications. GGA-PBE predicts higher mechanical strength and is more effective for studying band gap closure and optical absorption compared to LDA-CAPZ. $CsPbI_3$ is promising for solar energy devices due to its optical properties, while $CsPbCl_3$ and $CsPbBr_3$ are better for mechanically stable optoelectronic applications. Current research work findings support the potential of $CsPbM_3$ perovskites for practical applications as well as experimental validation.
Keywords: first-principles calculations, Halide perovskites, mechanical stability, band gap, optical response.

1. INTRODUCTION

In 1839, a mineral named ($CaTiO_3$) was discovered by the German geologist Gustav Rose in the Ural Mountains of Russia. Further research on this mineral was conducted by Russian mineralogist Count Lev Alexevich von Perovski. The material was given the name perovskite in recognition of his contributions. Over time, materials that resemble $CaTiO_3$ in structure have been categorized as perovskites [1]. The name now widely refers to any material with the same crystal lattice structure as $CaTiO_3$. Perovskites have the general formula ABX_3 [2]. Where A symbolizes a monovalent cation (e.g., Cs^+, MA^+, or FA^+), B represents a divalent metal cation (e.g., Pb^{2+}, Sn^{2+}), and X signifies a halide anion (e.g., F^-, Cl^-, Br^-, or I^-). Both theoretically and experimentally, perovskites show a variety of fascinating features. These materials are well-known for their enormous magneto-resistance, charge ordering, spin-dependent transport, superconductivity, ferroelectric behavior, and high thermoelectric power [3]. Additionally, they demonstrate a strong interaction between structural, magnetic, and optical properties [4]. Halide lead perovskite compounds have acquired popularity in light-driven catalysis due to their versatile absorption spectrum, affordability, and plentiful catalytic sites [5]. Inorganic perovskites have received a lot of scientific attention because they are more physically and chemically stable than organic perovskites. Among them, Cs-based $CsPbM_3$ (X =F, Cl, Br, I) is a potential material for the upcoming generation of electrical, optoelectronic, and other light-responsive technologies [6].To increase the proficiency of optoelectronic devices, including light emitting devices, photonic detectors and lasers, the properties of $CsPbM_3$ should be altered by introducing metal halides or merging them with halides [7]. The combination of low-cost production processes, excellent efficiency, and adjustable features has elevated lead perovskites to the leading edge of research, with the potential to profoundly impact energy technologies and optoelectronic devices in the near future. The bandgap tunability of lead perovskites enables their optimization for diverse applications, including efficient solar energy conversion and narrow-band light emission in LEDs. Our research intends to explore the electronic framework and optical characteristics of perovskite materials with the GGA-PBE functional and LDA-CAPZ functional. These functionals are mathematical models used in DFT to predict the exchange-correlation energy – a key feature in describing the electrical properties of materials. LDA is simpler and computationally efficient, but it frequently overbinds atoms and underestimates band gaps. GGA increases accuracy for structural and electronic properties while being somewhat more computationally demanding. These functionals enable us to explore the band

* Corresponding author: M.A. Javid
E-mail: *arshad.javid@iub.edu.pk*

structure, density of states, and optical response of the compounds in detail. This comparison helps to validate the accuracy of our approach and provides deeper insights into the properties of perovskites. Pressure has a significant influence on regulating the physical characteristics of materials [8, 9], allowing precise control over their optical, electrical, and optoelectronic properties as well as affecting phase transitions. The study of pressure-dependent features is especially important for quantum dot-based optoelectronic technologies, since high-pressure research gives crucial perspectives into the optoelectronic behavior of perovskite materials, notably photoluminescence dynamics. The ability to vary the E_g via pressure deviations increases the material's potential for optoelectronic devices by facilitating efficient electron transitions from the VB to the CB, maximizing photon absorption and electrical conduction.

2. COMPUTATIONAL METHODOLOGY

The space group of $CsPbM_3$ (where M = F, Cl, Br, I) is typically Pm-3m (space group number 221), corresponding to the cubic perovskite structure. The lattice constants (Å) of bulk perovskites of $CsPbM_3$ (M = F, Cl, Br, I) are 4.83, 5.68, 5.95 and 6.38 Å, respectively. DFT simulations were performed using Materials Studio 2020 with the CASTEP module to analyze the electrical structure and optical features of cubic perovskite $CsPbM_3$.The exchange-correlation interactions were calculated using the Generalized Gradient Approximation (GGA) with the Perdew-Burke-Ernzerhof (PBE) functional and the Local Density Approximation (LDA) with the Ceperley-Alder-Perdew-Zunger (CAPZ) parameterization. Geometry optimization was executed using Limited-memory Broyden-Fletcher-Goldfarb-Shanno (LBFGS) approach. Core electron effects were treated via On-the-Fly Generation (OTFG) ultrasoft pseudopotentials. Pseudo-atomic calculations were utilized for Cs ($5s^2\ 5p^6\ 6s^1$), Pb ($5s^2\ 5p^6\ 5d^{10}\ 6s^2\ 6p^2$) and M = F, Cl, Br, I ($ns^2\ np^5$ where n = 2, 3, 4 and 5 respectively). A 6×6×6 k-point mesh was used to integrate the Brillouin zone, and a threshold of 400 eV was applied for wavefunction expansion. The convergence criteria included an energy tolerance of 2.0×10^{-5} eV per atom, a maximum force tolerance of 0.05 eV/Å per atom, a maximum stress tolerance of 0.1 GPa, and a maximum ionic displacement of 0.002 Å.

The calculations were carried out under an external pressure of 10 GPa to investigate structural and electronic behavior under high pressure conditions since this hydrostatic pressure is not only accessible experimentally (through diamond anvil cells) but also in a regime where halide perovskites exhibit systematic structural compression and significant changes in electronic or optical behavior without causing irreversible structural collapse. As one example, Zhang et al. [10] report similar narrowing of the band-gap and optical shifts in $CsPbCl_3$ under similar compression. Similar structural and electronic changes in $CsPbX_3$ (X = I, Br, Cl) at pressures of less than approximately 10 – 20 GPa are observed by Wang et al. [11]. Moreover, the review work "Pressure responses of halide perovskites…" [12] demonstrates that numerous perovskite compounds display noticeable optoelectronic responses at around 10 GPa. Therefore, 10 GPa is a powerful benchmark pressure to our work, and it is both physically relevant, computationally feasible, and aligned with the literature.

3. RESULTS AND DISCUSSION

3.1. Mechanical properties

The mechanical characteristics of lead perovskites are critical to their performance and stability in solar cells, LEDs, and flexible electronics[13]. This study uses the stress-strain technique to derive the elastic constant tensor C_{ij} (Table 1).

Table 1. Pressure-dependent elastic constants (C_{ij}) in GPa calculated for $CsPbF_3$, $CsPbCl_3$, $CsPbBr_3$, and $CsPbI_3$

Compound	Method	C_{11}	C_{12}	C_{44}
$CsPbF_3$	PBE	81.157	-8.694	7.853
$CsPbCl_3$	PBE	55.624	9.188	5.088
$CsPbBr_3$	PBE	46.463	7.498	4.210
$CsPbI_3$	PBE	42.651	6.269	3.425
$CsPbF_3$	LDA	65.450	-14.67	8.068
$CsPbCl_3$	LDA	46.828	5.071	4.736
$CsPbBr_3$	LDA	38.810	3.674	3.978
$CsPbI_3$	LDA	34.971	2.463	3.394

The Voigt-Reuss-Hill approximation is applied to compute Bulk modulus of elasticity (B), shear modulus (G), and Poisson's ratio (v). The hardness (H) is obtained via Tian's model, and the C_{ij} are derived using the stress-strain technique. These are critical parameters that influence how a compound responds to variations in stress, strain, and temperature. Overall, improving mechanical qualities contributes to the reliability, long-term sustainability, and excellent performance of perovskite-based devices. Fig. 1 depicts the optimized cubic structures of $CsPbM_3$.

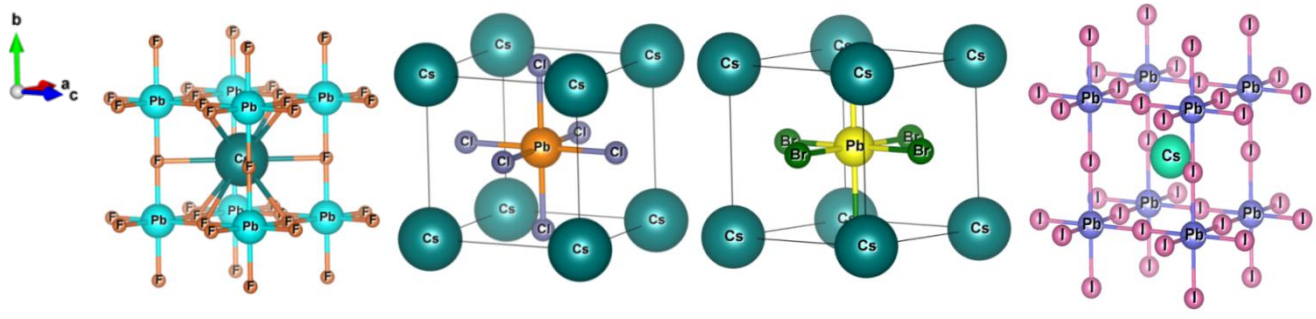

a b c d

Fig. 1. Crystal structures analysis of $CsPbM_3$ (M = F, Cl, Br, I) cubic Perovskites: a– $CsPbF_3$; b – $CsPbCl_3$; c – $CsPbBr_3$; d – $CsPbI_3$.

Although all compounds can crystallize in the ABX_3 perovskite structure using corner-sharing PbX_6 octahedra, $CsPbF_3$ and $CsPbI_3$ adopt an identical cubic structure, but $CsPbCl_3$ and $CsPbBr_3$ are found in a different but equivalent cubic structure.

The mechanical stability of all $CsPbM_3$ perovskites is confirmed by the fact that their elastic constants (C_{ij}) meet the following Born stability criteria:

$$C_{11} > 0, C_{44} > 0, C_{11} - C_{12} > 0, C_{11} + 2C_{12} > 0, C_{12} < C_{11}. \quad (1)$$

Table 1 illustrates that $CsPbCl_3$, $CsPbBr_3$, and $CsPbI_3$ are stable under pressure (10 GPa) using both PBE and LDA functionals. $CsPbF_3$ is stable in PBE but unstable in LDA due to a negative value of $C_{11}+2C_{12}$, suggesting mechanical instability under pressure [14]. The bulk modulus of elasticity (*B*), Young's modulus (*E*), shear modulus (*G*) and Poisson's ratio (*v*) can be computed using the following relationships.

$$B = \frac{C_{11} + C_{12}}{3}; \quad (2)$$

$$G = \frac{G_V + G_R}{2}; \quad (3)$$

$$G_V = \frac{(C_{11}-C_{12})+3C_{44}}{5}; \quad (4)$$

$$G_R = \frac{5(C_{11}-C_{12})C_{44}}{3(C_{11}-C_{12})+4C_{44}}; \quad (5)$$

Since

$$G_R \leq G \leq G_V; \quad (6)$$

The Young's modulus is given by:

$$E = \frac{9BG}{3B + G}; \quad (7)$$

and Poisson's ratio is:

$$\nu = \frac{3B-2G}{2(3B+G)}. \quad (8)$$

Bulk modulus that is used to measure the resistance of a given material to any uniform compression by an external pressure. It is defined as the applied pressure divided by the relative volume change. This represents a material's capacity to keep its structure when compressed. A higher bulk modulus suggests less compressibility and more structural stiffness, whereas a lower bulk modulus indicates increased compressibility. The mechanical properties of $CsPbM_3$ (M = F, Cl, Br, I) under 10 GPa external pressure, calculated using the PBE and LDA functionals, exhibit distinct trends in bulk modulus, shear modulus, and Young's modulus, reflecting the influence of ionic size, bond strength, and the specific characteristics of the functionals used. Earlier studies demonstrated that the properties concerning stiffness in lead halide perovskites are connected to the size of the halogen ion and the strength of the Pb-halogen bond [15, 16]. The PBE results show that the bulk modulus follows the trend of $CsPbCl_3$>$CsPbF_3$>$CsPbBr_3$>$CsPbI_3$, which is consistent with the inverse relationship between lattice constant and compressibility [17]. Smaller ions, which form stronger ionic connections, are more resistant to compression. LDA provides a distinct ordering because to its natural overbending property. This leads to shorter lattice constants and artificially stronger bonding, especially in $CsPbF_3$, leading to a lower bulk modulus. Compared to prior works [13, 18], which either neglected the effect of external pressure or were limited to organic or incomplete halide systems, our approach offers a more comprehensive and physically reliable perspective. Ji et al. [13] focus on hybrid perovskites at ambient pressure, while Ahmad et al. [18] exclude $CsPbF_3$ and show inconsistent mechanical trends due to their singular functional approach. Our findings correct these gaps by systematically evaluating all halides under pressure, yielding more reliable stiffness and hardness predictions. For shear modulus, both PBE and LDA predict the trend $CsPbF_3$>$CsPbCl_3$>$CsPbBr_3$>$CsPbI_3$, with $CsPbF_3$ demonstrating the strongest bonds and the greatest stiffness. Pugh's ratio (B/G) refers to the relationship between bulk modulus and shear modulus. Pugh suggests employing the B/G ratio to assess a material's plastic properties, including ductility and brittleness. Ductile materials are those with a Pugh's ratio more than 1.75 [19]. $CsPbCl_3$, $CsPbBr_3$, and $CsPbI_3$ have high *B*/*G* ratios (~2.49 – 2.57 in PBE), indicating ductility. $CsPbF_3$ is more brittle (*B*/*G* = 1.23 in PBE, 0.71 in LDA), consistent with prior results on fluorine-based perovskites under strain [20]. Young's modulus determines a material's stiffness by assessing its resistance to stretching or compressing under an applied force. A higher value suggests stronger stiffness and less deformation, whereas a lower value shows the material's flexibility and ease of deformation. The PBE functional calculations show that $CsPbF_3$ has the maximum stiffness and resistance to deformation, supporting previous theoretical and experimental work on perovskite elasticity [21]. The LDA functional data indicate a different ordering, with $CsPbF_3$ still having the greatest stiffness, but $CsPbBr_3$ outranking $CsPbCl_3$. LDA overestimates bonding strength, especially in $CsPbBr_3$, resulting in an exaggerated rise in stiffness, which is consistent with its known overbending tendencies [22]. $CsPbF_3$ demonstrates the strongest resistance to deformation and stiffness, whereas $CsPbI_3$ has the lowest mechanical strength. Poisson's ratio (*v*) indicates a crystal' stability against shear and inherent toughness. A value larger than 0.26 indicates relative toughness, whereas a lower value indicates brittleness. In PBE results the values suggest that $CsPbF_3$ is more brittle, and the other materials exhibit progressively more ductile behavior. Poisson's ratio (*v*), a measure of shear resistance and toughness, is >0.26 for all compounds except $CsPbF_3$, suggesting that the latter is more brittle. This also aligns with trends reported in other halide perovskite studies under external pressure [23].On the other hand, the LDA results show significantly lower Poisson's ratio for $CsPbF_3$ and slightly higher values for the others, reflecting LDA's tendency to overestimate bonding and distort material behavior, especially for $CsPbF_3$. Hardness is a material property that evaluates its resistance to localized plastic deformation, such as indentation or scratching. It denotes a material's capacity to tolerate mechanical forces without permanent deformation. The harder the substance, the more resistant it is to indentation or scratching, and is estimated by Tian empirical model [24]:

$$H = 2\left(\frac{G^3}{B^2}\right)^{0.585}. \quad (9)$$

An alternative model, proposed by Chen et al. [25], relates hardness to Pugh's ratio $K = G/B$ and shear modulus:

$$H = 0.92 \times K^{1.137} \times G^{0.708}. \quad (10)$$

PBE shows $CsPbF_3$ as the hardest material, with a hardness value of 5.421 GPa indicating its brittleness while $CsPbCl_3$, $CsPbBr_3$, and $CsPbI_3$ exhibit lower hardness values indicating more ductile behavior. However, LDA predicts much greater hardness for $CsPbF_3$ (9.726 GPa) than PBE, indicating an overestimate of its resistance to deformation. The hardness values for the other materials are likewise greater in LDA than in PBE, indicating that LDA's tendency to overbend leads to artificially stronger materials, distorting the projected mechanical characteristics. A further analysis of the chemical bonding evolution throughout the halide series is shown using the Mulliken population and energy analysis of a bond valence (Table 2). In the case of $CsPbF_3$, Pb-F bonds hold a low bond overlap population (0.08 – 0.17) and the short bond length is 2.415 Å, characteristic of mixed ionic-covalent nature and strong bond interactions, which is associated with high elastic moduli and brittle behavior. The bond population in $CsPbCl_3$ rises (~0.30 – 0.35), indicating greater covalency and stronger Pb-Cl bonds, which is in agreement with its moderate ductile behavior. In the case of $CsPbBr_3$, the population once more decreases (~0.08 – 0.17), which means a weaker covalency and softer bonds. The population of the Pb-I bonds becomes insignificant in $CsPbI_3$, indicating highly ionic and weak Pb-I bonding, which is why it is the least hard and a most ductile bond in the series. These results agree with Bond Valence Theory, in which bond valence sum (BVS) changes systematically *F* to *I* as the halide ionic radius and bond length increase. These microscopic changes in the bonding process directly define macroscopic properties: stronger Pb-F and Pb-Cl bonds enable more mechanical strength, and weaker Pb-Br and Pb-I bonds result in lower hardness and a smaller bandgap in line with the trend of the redshift with the absorption. Similar methodology is described in spinel oxides ($ZnO{\cdot}nAl_2O_3$) in which bond population and BVS analyses were employed to justify property trends [33].

3.2. Electronic properties

In photovoltaic and optoelectronic applications, materials' electronic characteristics are critical because they directly impact how the material interacts with light and conducts electricity. To determine how a material will perform in various applications, it is necessary to investigate its energy band gap, which governs how quickly electrons may travel from the valence band (where electrons are typically found) to the conduction band (where electrons can move freely). Table 3 shows how the PBE and LDA functions were used to calculate the E_g for various $CsPbM_3$ structures. Fig. 2 and Table 3 show that increasing the halogen size (from F to I) leads to higher optimized lattice constants and lower band gap energy for the compounds. This is consistent with previous investigations on perovskite materials [34, 35]. In essence, by using various halogens, you may modify the structural and electrical characteristics of perovskite materials. This versatility makes them excellent for use in photovoltaics, optoelectronics, and photodetectors. Furthermore, LDA has lower lattice constants than PBE due to its greater electron binding, resulting in a more compact structure. LDA gives narrower band gaps than PBE, as predicted, because LDA results in an underestimated band gap by overbending electrons [36]. Both approaches show a strong correlation between halogen size and lattice expansion under pressure. The calculated band gaps for four structures follow the almost identical trends $CsPbF_3$>$CsPbCl_3$>$CsPbBr_3$>$CsPbI_3$, consistent across both PBE and LDA methods, though the values differ. The PBE-calculated band gaps are 2.629 eV, 2.110 eV, 1.695 eV, and 1.303 eV, respectively (Fig. 2 a – d), whereas LDA gives 2.498 eV, 1.904 eV, 1.540 eV, and 1.280 eV, respectively (Fig. 2 e – h). At the R-symmetry point, all of the investigated materials act as semiconductors with a direct band gap. This significant difference in results suggests that PBE functional is the most appropriate approach for precisely calculating the electronic properties of these materials, as its values are in closer agreement with the experimental literature.

Table 2. Calculated pressure-dependent mechanical characteristics of the material

Materials	Bulk modulus, GPa	Shear modulus, GPa	Young's modulus, GPa	Poisson's ratio, GPa	Hardness, GPa	*B*/*G*	Pb-X bond population	Pb-X bond length, Å
	GGA-PBE							
$CsPbF_3$	21.255	17.202	40.643	0.181	5.421	1.23	0.08	2.415
$CsPbCl_3$	24.667	9.870	26.126	0.323	1.642	2.49	0.35	2.840
$CsPbBr_3$	20.486	8.226	21.766	0.322	1.449	2.49	0.17	2.975
$CsPbI_3$	18.566	7.201	19.131	0.328	1.268	2.57	Negligible	–
	LDA-CAPZ							
$CsPbF_3$	11.708	16.352	33.474	0.023	9.726	0.71	0.17	2.415
$CsPbCl_3$	18.990	9.024	12.973	0.294	1.874	2.10	0.30	2.840
$CsPbBr_3$	15.386	7.587	19.550	0.288	1.729	2.02	0.08	2.975
$CsPbI_3$	13.229	6.752	17.324	0.282	1.645	1.95	Negligible	–

Table 3. The optimized lattice parameters, unit cell volumes, and band gap values for $CsPbF_3$ $CsPbCl_3$, $CsPbBr_3$, and $CsPbI_3$ calculated under pressure

Materials	P, GPa	Lattice constant, Å			Unit cell volume, V/Å^3		Band gap, eV			Bulk type
		PBE	LDA	Exp.	PBE	LDA	PBE	LDA	Exp.	
$CsPbF_3$	10	4.68	4.55	4.79 [26]	102	94	2.629	2.498	3.68 [27]	Cubic
$CsPbCl_3$	10	5.26	5.14	5.62 [18]	145	136	2.110	1.904	2.90 [28]	Cubic
$CsPbBr_3$	10	5.46	5.35	5.87 [29]	162	152	1.695	1.540	2.30 [30]	Cubic
$CsPbI_3$	10	5.74	5.61	6.28 [31]	189	177	1.303	1.280	1.70 [32]	Cubic

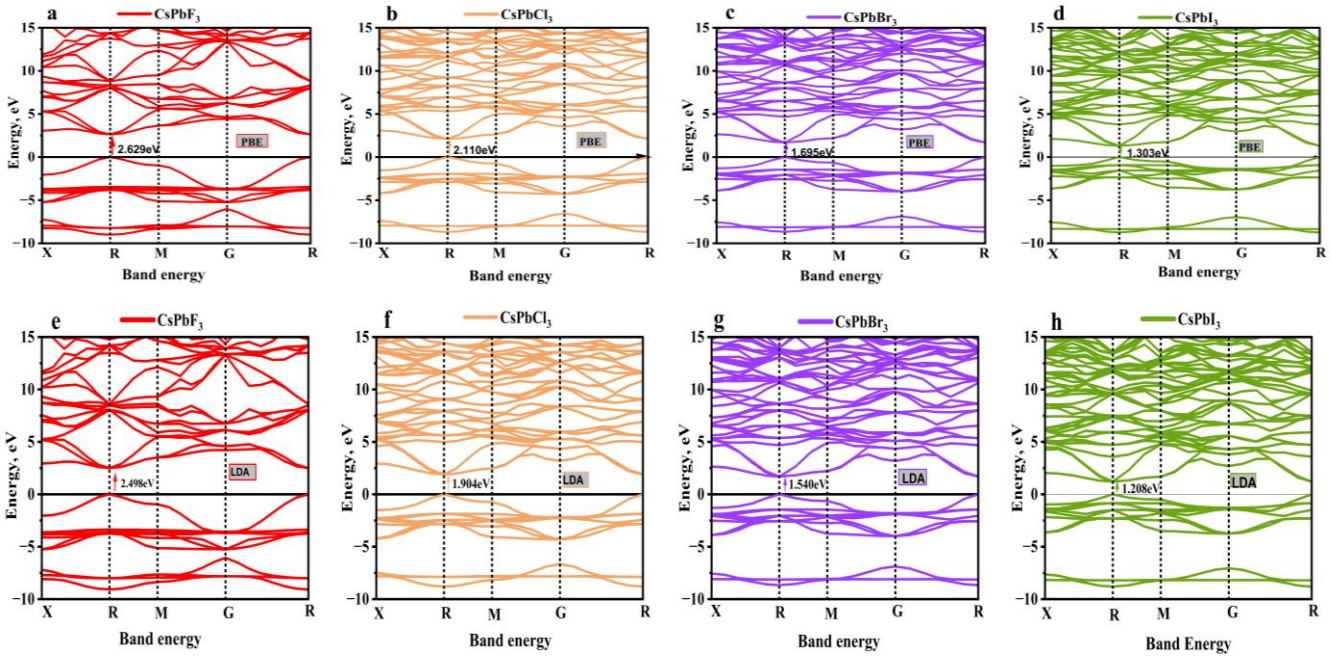

Fig. 2. The electronic band structures: a, b, c, d – computed using PBE method; e, f, g, h – computed using LDA method with applied pressure

The density of states (DOS) is a more accurate description of the bandgap. Fig. 2, shows the PDOS for four structures. The PDOS for $CsPbM_3$ (M = F, Cl, Br, I) is illustrated from -10 eV to 10 eV, with the Fermi level (E_F) placed at 0 eV. In the valance band (Fig. 3 a), the DOS peaks at 17.3 states/eV for $CsPbF_3$, 14.03 for $CsPbCl_3$, 13.2 states/eV for $CsPbBr_3$ and 11.7 states/eV for $CsPbI_3$. In the valence band (Fig. 3 b), $CsPbF_3$ has the highest DOS values at 18.2 states/eV, followed by $CsPbCl_3$ at 13.6, CsPbBr3 at 12.9 and CsPbI3 at 11.6. The absence of considerable overlap at E_f demonstrates that these compounds are semiconducting, as the E_V and E_B are well separated. This separation leads to the creation of the band gap. The CB is essentially made up of Cs and Pb orbitals, whereas the VB is dominated by halogen orbitals (F, Cl, Br, I). The thickness of the band gap is different depending on the halogen element due to the extent of orbital dispersion. Because the compounds separate with a gap at the Fermi level, all of them are considered semiconductors rather than metals. The flexible electronic properties indicate that gap size in $CsPbM_3$ can be adjusted by swapping halides, making them suited for solar energy and optoelectronic use. Research on band gap engineering is well documented and we find our results agree with these studies, along with pointing out the effects of pressure and the choice of functional group [37]. $CsPbF_3$, 14.03 for $CsPbCl_3$, 13.2 states/eV for CsPbBr3 and 11.7 states/eV for CsPbI3. In the valence band (Fig. 3 b), $CsPbF_3$ has the highest DOS values at 18.2 states/eV, followed by $CsPbCl_3$ at 13.6, CsPbBr3 at 12.9 and CsPbI3 at 11.6.

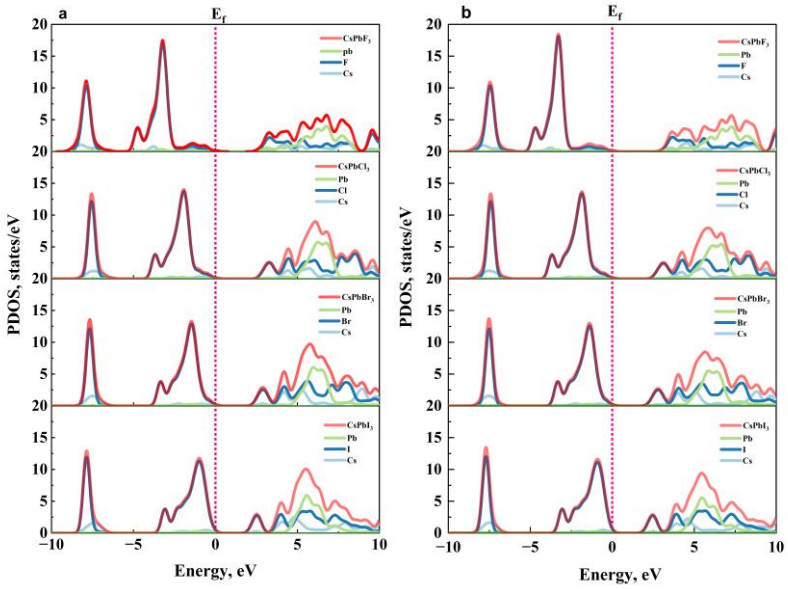

Fig. 3. Pressure-dependent PDOS of $CsPbF_3$, $CsPbCl_3$, $CsPbBr_3$, and $CsPbI_3$, computed using (a) PBE and (b) LDA method.

The absence of considerable overlap at E_f demonstrates that these compounds are semiconducting, as the E_V and E_B are well separated. This separation leads to the creation of the band gap. The CB is essentially made up of Cs and Pb orbitals, whereas the VB is dominated by halogen orbitals (F, Cl, Br, I). The thickness of the band gap is different depending on the halogen element due to the extent of orbital dispersion. Because the compounds separate with a gap at the Fermi level, all of them are considered semiconductors rather than metals. The flexible electronic properties indicate that the gap size in $CsPbM_3$ can be adjusted by swapping halides, making them suited for solar energy and optoelectronic use. Research on band gap engineering is well documented, and we find our results agree with these studies, along with pointing out the effects of pressure and the choice of functional group [37].

3.3. Optical properties

The optical characteristics of a material must be evaluated in order to determine its possible uses. This section analyzes the optical properties of the perovskite's materials $CsPbM_3$ (M = halides) with PBE and LDA. The optical behavior depends on the band gap and charge transporters in the valence and conduction bands. Furthermore, optical characteristics describe how a material responds to electromagnetic radiation. This is especially crucial for developing materials with certain optical properties, such as high transparency, strong absorption, or efficient light emission. The dielectric function is an important consideration in this analysis. It defines how the material responds to an external electromagnetic field and influences optical properties, including refractive index, absorption coefficient, and reflectivity. Mathematically, the real part $\varepsilon_1(\omega)$ and the imaginary part $\varepsilon_2(\omega)$ depict the dielectric function.

$$\varepsilon(\omega) = \varepsilon_1(\omega) + i\varepsilon_2(\omega). \quad (11)$$

In many first-principles computations (e.g., employing density functional theory), the imaginary component is computed as a sum of electronic transitions:

$$\varepsilon_2(\omega = \frac{2\pi e^2}{\Omega\varepsilon_0} \sum_{k,v,c} |\langle\psi_{ck}|\hat{e}.r|\rangle\psi_{vk}|^2 \delta(E_{ck} - E_{vk} - \hbar\omega) \quad . \quad (12)$$

$$\varepsilon_1(\omega) = 1 + \frac{2}{\pi} P \int_0^{\infty} \frac{\omega' \varepsilon_2(\omega')}{\omega'^2 - \omega^2} d\omega. \quad (13)$$

The complex refractive index correlates with the $\varepsilon(\omega)$ as follows:

$$\tilde{n}(\omega) = n(\omega) + ik(\omega) = \sqrt{\varepsilon(\omega)}. \quad (14)$$

At normal incidence, reflectivity $R(\omega)$ is calculated as:

$$R(\omega) = \left|\frac{\tilde{n}(\omega)-1}{\tilde{n}(\omega)+1}\right|^2 = \left|\frac{n(\omega)+i\,k(\omega)-1}{n(\omega)+ik(\omega)+1}\right|^2. \quad (15)$$

The absorption coefficient is associated to the extinction coefficient by:

$$\alpha(\omega) = \frac{2\omega k(\omega)}{C}. \quad (16)$$

The dielectric function is correlated to the frequency-dependent optical conductivity $\sigma(\omega)$:

$$\sigma(\omega) = \frac{i\omega}{4\pi}[\varepsilon(\omega) - 1]. \quad (17)$$

The energy loss function is the most crucial aspect of electron energy loss spectroscopy (EELS), and is given as:

$$L(\omega) = \mathrm{Im}\left[-\frac{1}{\varepsilon(\omega)}\right] \quad (18)$$

Fig. 4 a and b presented pressure dependent $\varepsilon_1(\omega)$and $\varepsilon_2(\omega)$ curves of $CsPbM_3$ with energy. The Peaks of ε_1 and ε_2 are found in the low energy region ($\leq$ 17 eV). In the high energy region (> 17 eV), ε_1 approaches 1 and ε_2 goes to 0, suggesting less absorption and behavior similar to a non-interacting dielectric [6]. Frequency-dependent $\varepsilon_1(\omega)$ varies with the applied frequency of the external electric field. At very low frequencies (approaching zero), the material may respond to the field more efficiently, which is captured by $\varepsilon_1(0)$. The $\varepsilon_1(0)$ represent the electronic contribution to the static dielectric constant. Table 4 shows our computed $\varepsilon_1(0)$ for $CsPbM_3$ (M = F, Cl, Br, I). The table shows that as you progress from F to I, there are rises. The relationship between E_g and $\varepsilon_1(0)$ is inverse, i-e E_g falls, the static dielectric constant rises [38]. The $\varepsilon_1(\omega)$ rises from $\varepsilon_1(0)$, reaches a maximum, then goes down and becomes negative at specified energy ranges. Within these regions, the incoming photon beam is entirely absorbed, which indicates high absorption or plasmonic activity. Moreover, the negative values of the $\varepsilon_1(\omega)$ in the UV region for the four studied compounds suggest that these materials exhibit metallic characteristics in this energy range. As for $\varepsilon_2(\omega)$, indicating absorption behavior of the compounds.

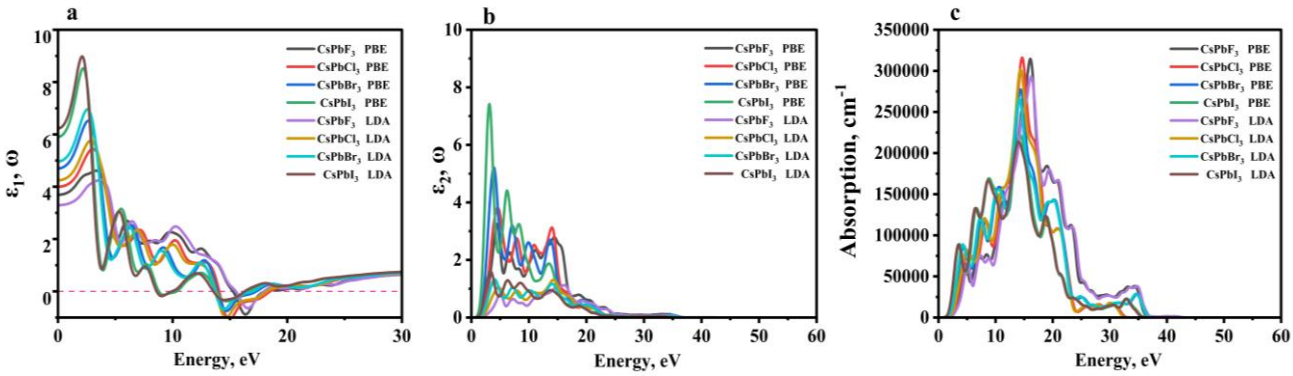

Fig. 4. Optical characteristics of cubic $CsPbM_3$ (M = F, Cl, Br, I): a – real part of dielectric function, $\varepsilon_1(\omega)$; b – imaginary part of dielectric function, $\varepsilon_2(\omega)$; c – absorption coefficient, $\alpha(\omega)$

High-quality optical materials absorb photons almost totally on the top surface. The values match those calculated from electrical band structures and are closely related to the optical bandgap. During prior optical studies on perovskites, researchers observed a link between $\varepsilon_2(\omega)$ and the optical bandgap [39]. Applying pressure increased the $\varepsilon_2(\omega)$, shifting the peaks towards lower incident photon energy. On the other hand, photon energy increased, $\varepsilon_2(\omega)$ dropped to zero. The maximum peaks observed in PBE functional are 3.24 eV for $CsPbF_3$, 3.66 eV for $CsPbCl_3$, 5.21 eV for $CsPbBr_3$ and 7.39 eV for $CsPbI_3$. However, LDA functional offers maximum peaks for $CsPbF_3$ at 0.77 eV, $CsPbCl_3$ at 1.04 eV, $CsPbBr_3$ at 1.29 eV and for $CsPbI_3$ at 1.6 eV. The higher maximum peaks in the $\varepsilon_2(\omega)$ indicate higher optical absorption. The peaks observed using PBE Functional reflect the material's stronger absorption at specific photon energies than LDA Functional, often due to higher transition probabilities between electronic states. Aktary et al. [6]. have described pressure-dependent narrowing of the band gap and increased dielectric in $CsPbCl_3$, $CsPbBr_3$, and $CsPbI_3$, which are similar trends to those observed in our calculated pressure-dependent optical responses. Fig. 4 c illustrates how the optical absorbance of $CsPbM_3$ perovskites varies with pressure. The graph shows how the absorption coefficient increases when bigger ionic radius halogen atoms are substituted. The absorption peaks of the corresponding materials exhibit the optical band gaps as E_g ($CsPbF_3$)>E_g ($CsPbCl_3$)>E_g ($CsPbBr_3$)>E_g ($CsPbI_3$), which coincides with the estimated values of E_g of $CsPbM_3$ perovskites (Table 3). This trend, like previous work by [40], demonstrates how heavier halide substitution leads the band gap in lead halide perovskites to decrease. Absorption coefficient (α) illustrates strong peaks around 3 – 5 eV, 8 – 12 eV, and 15 – 20 eV, indicating strong absorption occurs at these energies.

The refractive index is a complex function with real and imaginary components denoted by $n(\omega)$ and $K(\omega)$, also known as the extinction coefficient. The extinction coefficient quantifies the absorption of electromagnetic radiation by matter. Refractive index is a fundamental optical property that governs how light disperses within a material. Its significance extends across multiple advanced technologies, including Solar Cells Infrared Sensors Optical Waveguides Photonic Crystals. Understanding and adapting enables scientists and engineers to improve device performance, increase energy efficiency, and create next-generation photonic technologies. Fig. 5 a and b shows refractive index results. The results in Table 4 show that the computed $n(\omega)$ at $n(0)$ rises from F to I. The refractive indices of these materials rise from zero-frequency to their peak values.

Table 4. Zero-frequency limits of $\varepsilon_1(\omega)$, $n(\omega)$ and $R(\omega)$

Compound	Method	$\varepsilon(0)$	$n(0)$	$R(0)$
$CsPbF_3$	PBE	3.69	1.92	0.10
$CsPbCl_3$	PBE	4.00	2.00	0.11
$CsPbBr_3$	PBE	4.70	2.18	0.13
$CsPbI_3$	PBE	5.92	2.44	0.17
$CsPbF_3$	LDA	3.29	1.81	0.08
$CsPbCl_3$	LDA	4.25	2.06	0.12
$CsPbBr_3$	LDA	4.97	2.23	0.14
$CsPbI_3$	LDA	6.23	2.50	0.18

Above these maximum values, the refractive index begins to reduce and, in specific energy ranges, falls under unity (less than one). Materials having refractive index values ranging from 2.0 to 4.0 are commonly used in optoelectronic applications. The materials investigated in this study fall within this range, indicating their potential for optical device fabrication. Furthermore, the refractive index values are larger than one, which strongly shows that these materials are semiconductors. Between 3.0 eV and 20 eV, the total system continues to decline with increasing photon energy, and the curves practically overlap until 36 eV, whereupon the refractive index of the system renders to be effectively fixed at about 0.96. The energy band gap (E_g) and the refractive index (n) have an inverse relationship. A narrower band gap produces a higher refractive index, and vice versa, which is consistent with reported trends in halide perovskites [41]. LDA often predicts narrower band gaps than PBE, which should result in a higher refractive index in most circumstances. Fig. 4 b shows extinction curve, as frequency increases the values of $k(\omega)$ decreases, and all materials show several peaks owing to resonances at different energy levels, as in previous DFT studies[42]. The results acquired using the PBE and LDA functionals exhibit that $CsPbI_3$ has the greatest $k(\omega)$ of the four compounds, suggesting strong optical interactions. $CsPbBr_3$ and $CsPbCl_3$ exhibit similar trends, but have slightly lower refractive index values. $CsPbF_3$ has the lowest refractive index, which correlates with its bigger bandgap and lower polarizability. The LDA functional often predicts greater peak values for the refractive index compared to PBE.

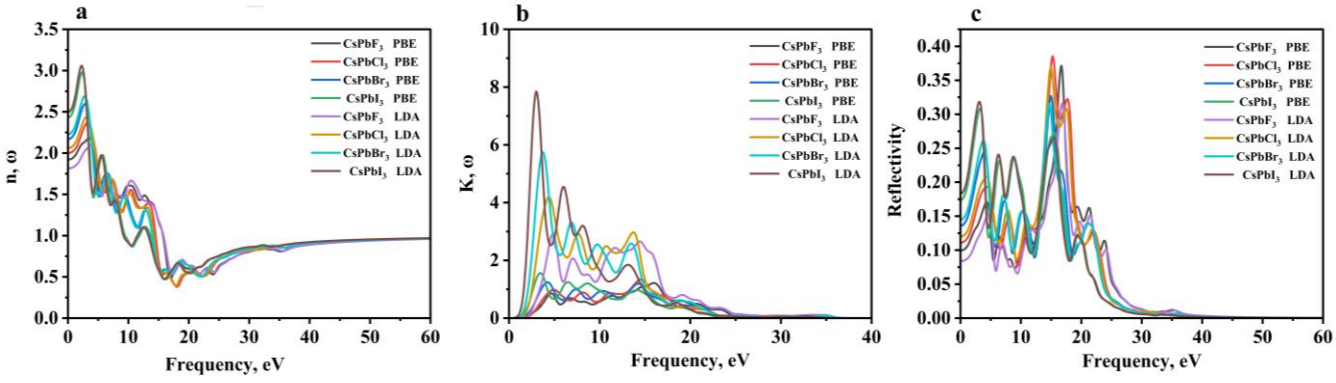

Fig. 5. The real and imaginary components of refractive Index and reflection for $CsPbM_3$ (M = F, Cl, Br, I).

At frequency above ~20 eV, extinction coefficient approaches zero for all materials, indicating a feeble optical response. Extinction coefficient also has peaks at the same places since $k(\omega)$ is directly proportional to and $\varepsilon_2(\omega)$, but with varying magnitudes.

$$\varepsilon_2=2nk. \quad (19)$$

Thus, when $\varepsilon_2(\omega)$ is large $k(\omega)$ rises, confirming their theoretical relationship. The variation in peaks between LDA and PBE is related to bandgap variations and how each functional tackles electronic transitions' figures out greater refractive index peaks, indicating stronger polarization effects, whereas PBE predicts higher direct absorption losses. Reflectivity graph (Fig. 5 c) uses both PBE and LDA functionals to illustrate how optical reflectance changes with photon energy for $CsPbM_3$ (X = F, Cl, Br, I) perovskites at 10 GPa pressure. Reflectivity tends to rise as a material's metallic character increases, which is associated with the negative $\varepsilon_1(\omega)$ value. The reflectance at zero frequency indicates each perovskite's static optical response. PBE and LDA functionals exhibit comparable patterns (Table 4), but LDA significantly overestimates R(0) for Cl, Br, and I. Heavy halides (Br, I) exhibit higher reflectivity at low frequencies due to narrower band gaps. Lighter halides (F, Cl) have lower reflectivity due to wider band gaps. $CsPbI_3$ has the greatest R(0), indicating it is highly reflective at low frequencies. $CsPbF_3$ has the lowest R(0), suggesting a poor static optical response. Optical conductivity is an important property in optoelectronic materials because it affects how well a material interacts with light and conducts photo-excited charge carriers. Solar cells, LEDs, photodetectors, and lasers are all affected by optical conductivity, which has a considerable impact on their efficiency and functioning. Fig. 6 a and b depicts the real (Re) and imaginary (Im) components of photoconductivity. High optical conductivity at low frequencies indicates considerable absorption, whereas low conductivity at high frequencies enables transparency in the UV or visible ranges. Materials with moderate optical conductivity can establish a balance between absorption and transparency, which is vital for display technologies and optical coatings. Both PBE and LDA functionals show peaks in low-energy (~3 – 8 eV) and high-energy (~10 – 15 eV) regions. $CsPbI_3$, $CsPbBr_3$, and $CsPbCl_3$ show peaks in both low-energy and high energy regions, while $CsPbF_3$ has its significant response in the 10 – 15 eV range, making it is less effective for visible and near-IR applications but more active in the deep UV range. $CsPbI_3$ is ideal for solar cells and photodetectors, while $CsPbF_3$ may be more beneficial in UV-transparent coatings or insulating layers. The energy loss function (Fig. 6 c) in your graph shows the dissipation of energy from plasmonic excitations in $CsPbM_3$ (X = F, Cl, Br, I) perovskites. The strongest peak is found at 18 – 22 eV for all substances. $CsPbCl_3$ (PBE) exhibits the largest peak, suggesting the strongest plasmon resonance and probably the highest free-electron density in this range. $CsPbF_3$ and $CsPbI_3$ have slightly smaller peaks, indicating reduced plasmonic activity. All materials exhibit a quick reduction in the loss function at 30 eV, suggesting the end of considerable plasmonic activity. Materials exhibiting stronger plasmonic peaks, such as $CsPbCl_3$ and $CsPbBr_3$, may be more suitable for high-frequency optoelectronic applications, including plasmonic-based solar cells or optical sensors. $CsPbI_3$'s wider loss function predicts superior performance in infrared/visible light absorption applications, including photodetectors. PBE predicts significantly stronger plasmon peaks than LDA, which is consistent with trends in reflectivity and photoconductivity. LDA underestimates energy loss, which is associated with its overall tendency to underestimate electronic excitations.

4. CONCLUSIONS

This systematic investigation enabled the study of halide perovskites through Density Functional Theory (DFT), incorporating GGA-PBE and LDA-CAPZ functionals to study pressure-dependent mechanical, electronic, and optical characteristics of cubic $CsPbM_3$ (M = F, Cl, Br, I) perovskites. Confirmation of mechanical stability up to 10 GPa and identification of the stiffest among them being $CsPbF_3$ yield new insights into the structural stability in high-pressure situations – an uncharted territory so far for halide perovskites. Electronic structure research provided systematic band gap reduction from $CsPbF_3$ to $CsPbI_3$, proving electronic properties can be effectively controlled by halide substitution. This control is key to maximizing materials for particular electronic and optoelectronic uses. Optical research showed intense UV-visible light absorption with red-shifted absorption edges rising with increasing halogen size. Dielectric function (ε_1 and ε_2) trend, refractive index, and extinction coefficient in various halides unveiled richness in trends in line with electronic structure, portraying a richer overview of light-matter interaction within the materials.

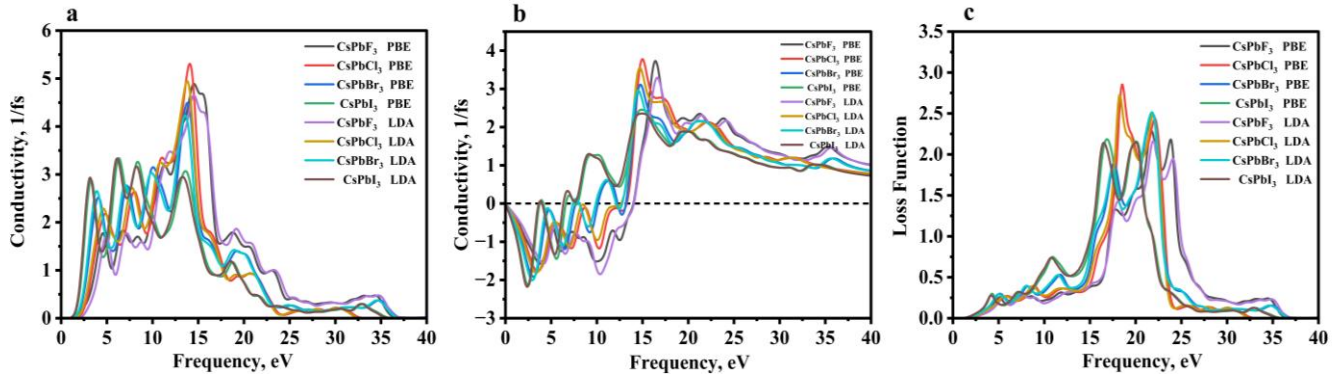

Fig. 6. The optical conductivity and loss function for $CsPbM_3$ (M = F, Cl, Br, I).

Notably, the LDA functional was found to take higher polarization effects into account, with PBE having more straight-forward optical transitions, uncovering relative insight into methodology impact on optical prediction. In addition, photoconductivity and energy loss spectra have set up $CsPbCl_3$ and $CsPbI_3$ as promising materials for higher optical conductivity and plasmonic activity and thus proposed their application in photonic and optoelectronic devices. Increased reflectance at heavier halides – owing to smaller band gaps – only facilitates their application in optical coatings or reflecting elements.

By intense investigation of the relationship between pressure, halide composition, and physical properties, this research develops the current state of knowledge of halide perovskites at non-atmospheric pressure. The findings not only demonstrate pressure as a useful tool to control material performance, but also provide the theoretical basis for future design and optimization of $CsPbM_3$-based perovskites for microelectronics, photovoltaics, and high-performance optoelectronic devices. Thus, this study significantly contributes to the growing body of literature on functional materials by addressing the previously underexplored pressure-induced property modulation in cubic halide perovskites.

REFERENCES

1. **Lamichhane, A.** First-Principles Density Functional Theory Studies on Perovskite Materials. New Jersey Institute of Technology, PhD thesis, 2021: pp. 1 – 150. https://digitalcommons.njit.edu/dissertations/1518/
2. **Tanaka, H., Misono, M.** Advances in Designing Perovskite Catalysts *Current Opinion in Solid State and Materials Science* 5 (5) 2001: pp. 381-387. https://doi.org/10.1016/s1359-0286(01)00035-3
3. **Kot, M., Wolska-Pietkiewicz, M., Pańczyk, T., Okal, J.** Perovskites: From Materials Science to Devices *Journal of Materials Chemistry C* 12 (28) 2024: pp. 10244 – 10245. https://doi.org/10.1039/d4tc90109f
4. **Murtaza, G., Ahmad, I., Maqbool, M., Jamil, M.** Investigation of Structural and Optoelectronic Properties of $BaThO_3$ *Optical Materials* 33 (3) 2011: pp. 553 – 557. https://doi.org/10.1016/j.optmat.2010.10.052
5. **Schanze, K.S., Castellano, F.N., Yang, P., Bisquert, J.** Progress in Perovskite Photocatalysis *ACS Energy Letters* 5 (10) 2020: pp. 2602 – 2604. https://doi.org/10.1021/acsenergylett.0c01480
6. **Aktary, M., Kamruzzaman, M., Afrose, R.** Pressure-Dependent Comparative Study of the Mechanical, Electronic, and Optical Properties of $CsPbX_3$ (X = Cl, Br, I): A DFT Study for Optoelectronic Applications. *Materials Advances* 4 (19) 2023: pp. 4494 – 4508. https://doi.org/10.1039/d3ma00311f
7. **Zhou, Y., Chen, J., Bakr, O.M., Mohammed, O.F.** Metal-Doped Lead Halide Perovskites: Synthesis, Properties, and Optoelectronic Applications *Chemistry of Materials* 30 (19) 2018: pp. 6589 – 6613. https://doi.org/10.1021/acs.chemmater.8b03297
8. **Coduri, M., Stroppa, A., Malavasi, L.** Origin of Pressure-Induced Band Gap Tuning in Tin Halide Perovskites *Materials Advances* 1 (8) 2020: pp. 2840 – 2845. https://doi.org/10.1039/d0ma00525c
9. **Kholil, M., Bhuiyan, M.** Effects of Pressure on Narrowing the Band Gap, Visible Light Absorption, and Semi-Metallic Transition of Lead-Free Perovskite $CsSnBr_3$ for Optoelectronic Applications *Journal of Physics and Chemistry of Solids* 154 2021: pp. 110083. https://doi.org/10.1016/j.jpcs.2021.110083
10. **Zhang, L., Liu, T., Xu, H., Wang, W., Yu, W.** Pressure-Induced Structural Evolution and Optical Properties of Metal-Halide Perovskite $CsPbCl_3$ *The Journal of Physical Chemistry C* 122 (27) 2018: pp. 15220 – 15225. https://doi.org/10.1021/acs.jpcc.8b05397
11. **Wang, X., Meng, W., Liao, W., Wang, J., Yan, Y.** Pressure Effects on the Structures and Electronic Properties of Halide Perovskite $CsPbX_3$ (X = I, Br, Cl) *Physical Chemistry Chemical Physics* 23 (5) 2021: pp. 3479 – 3484. https://doi.org/10.1039/d0cp05892k
12. **Li, M., Guo, Y., Pan, Y., Chen, W.** Pressure Responses of Halide Perovskites with Various Compositions, Dimensionalities, and Morphologies *Matter and Radiation at Extremes* 5 (1) 2020: pp. 018401. https://doi.org/10.1063/1.5133653
13. **Ji, L.J., Zhao, Y.X., Wang, R., Gao, F.** Mechanical Properties of Hybrid Organic-Inorganic Perovskites *Coordination Chemistry Reviews* 391 2019: pp. 15 – 29. https://doi.org/10.1016/j.ccr.2019.03.020
14. **Slimani, R., Othmani, A., Khenata, R., Abidri, B., Ameri, M., Reshak, A.H.** Insights on Structural, Elastic, Electronic and Optical Properties Under Pressure of Cs-Based Fluoroperovskite $CsMF_3$ (M = Ge, Sn, Pb) Compounds *Computational Condensed Matter* 30 2024: pp. e00980. https://doi.org/10.1016/j.cocom.2024.e00980
15. **Ezzeldien, M., Abdel-Hady, F., Ghoneim, A., Alahmed, Z., Ashour, A.** Electronic and Optical Properties of Bulk and Surface of $CsPbBr_3$ Inorganic Halide Perovskite: A First Principles DFT-½ Approach *Scientific Reports* 11 (1) 2021: pp. 20622. https://doi.org/10.1038/s41598-021-99551-y
16. **Ghaithan, H.M., Ahmed, N.M., Al-Mashhadani, M.H., Alfaify, S., Khenata, R.** Structural, Electronic, and Optical Properties of $CsPb(Br_{1-x}Cl_x)_3$ Perovskite: First-Principles Study with PBE–GGA and mBJ–GGA Methods *Materials* 13 (21) 2020: pp. 4944. https://doi.org/10.3390/ma13214944
17. **Ghaithan, H.M., Alfaify, S., Reshak, A.H., Khenata, R.** Electronic Structure and Optical Properties of Inorganic Pm3m and Pnma $CsPbX_3$ (X = Cl, Br, I) Perovskite: A Theoretical Understanding from Density Functional Theory Calculations *Materials* 16 (18) 2023: pp. 6232. https://doi.org/10.3390/ma16186232
18. **Ahmad, M., Amin, N., Akhtar, F., Alam, M.** Structural, Electronic and Optical Properties of $CsPbX_3$ (X = Cl, Br, I) for Energy Storage and Hybrid Solar Cell Applications *Journal of Alloys and Compounds* 705 2017: pp. 828 – 839. https://doi.org/10.1016/j.jallcom.2017.02.147
19. **Pugh, S.** XCII. Relations Between the Elastic Moduli and the Plastic Properties of Polycrystalline Pure Metals *The London, Edinburgh, and Dublin Philosophical Magazine and Journal of Science* 45 (367) 1954: pp. 823 – 843. https://doi.org/10.1080/14786440808520496
20. **Yao, Z.Q., Huang, N., Fu, R.K.Y., Leng, Y.X., Chen, J.Y., Wang, J., Chu, P.K.** Structural, Mechanical and Hydrophobic Properties of Fluorine-Doped Diamond-Like Carbon Films Synthesized by Plasma Immersion Ion Implantation and Deposition (PIII–D) *Applied Surface Science* 230 (1 – 4) 2004: pp. 172 – 178.

https://doi.org/10.1016/j.apsusc.2004.02.044

21. **Mohammed, Z.Y., Sami, S.A., Salih, J.M.** First-Principles Calculation of Structural, Electronic, and Optical Properties of Cubic Perovskite $CsPbF_3$ *East European Journal of Physics* 3 2023: pp. 263 – 270. https://doi.org/10.26565/2312-4334-2023-3-23
22. **Ghaithan, H.M., Alfaify, S., Khenata, R., Reshak, A.H.** Density Functional Study of Cubic, Tetragonal, and Orthorhombic $CsPbBr_3$ Perovskite *ACS Omega* 5 (13) 2020: pp. 7468 – 7480. https://doi.org/10.1021/acsomega.0c00197
23. **Zaidi, S.J., Hussain, A., Khan, M., Ahmed, F., Iqbal, Z.** A Comparative DFT Assessment of the Mechanical, Elastic, Electronic, and Optical Parametric Study of Perovskites $CsPbX_3$ for Opto-Electronic Applications *Digest Journal of Nanomaterials and Biostructures* 19 (3) 2024: pp. 897 – 908. https://doi.org/10.15251/djnb.2024.193.1227
24. **Tian, Y., Xu, B., Zhao, Z.** Microscopic Theory of Hardness and Design of Novel Superhard Crystals *International Journal of Refractory Metals and Hard Materials* 33 2012: pp. 93 – 106. https://doi.org/10.1016/j.ijrmhm.2012.02.021
25. **Chen, X.Q., Niu, H., Li, D., Li, Y.** Modeling Hardness of Polycrystalline Materials and Bulk Metallic Glasses *Intermetallics* 19 (9) 2011: pp. 1275 – 1281. https://doi.org/10.1016/j.intermet.2011.03.026
26. **Berastegui, P., Hull, S., Eriksson, S.** A Low-Temperature Structural Phase Transition in $CsPbF_3$ *Journal of Physics: Condensed Matter* 13 (22) 2001: pp. 5077 – 5088. https://doi.org/10.1088/0953-8984/13/22/305
27. **Yan, X., Li, X., Wang, J., Zhou, Y., Wu, Y.** Growth and Characterization of All-Inorganic Halide Perovskite $CsPbF_3$ Single Crystals *Crystals* 13 (5) 2023: pp. 765. https://doi.org/10.3390/cryst13050765
28. **Zhu, Z., Bai, Y., Liu, X., Chueh, C.C., Yang, S., Jen, A.K.Y.** Antisolvent-Induced Fastly Grown All-Inorganic Perovskite $CsPbCl_3$ Microcrystal Films for High-Sensitive UV Photodetectors *Advanced Materials Interfaces* 8 (6) 2021: pp. 2001812. https://doi.org/10.1002/admi.202001812
29. **López, C.A., Briones, F., Ávila, J., Castellanos-Gomez, A.** Crystal Structure Features of $CsPbBr_3$ Perovskite Prepared by Mechanochemical Synthesis *ACS Omega* 5 (11) 2020: pp. 5931 – 5938. https://doi.org/10.1021/acsomega.9b04248
30. **Yuan, H., Zhao, J., Duan, J., Li, G., Yang, X.** All-Inorganic $CsPbBr_3$ Perovskite Solar Cell with 10.26% Efficiency by Spectra Engineering *Journal of Materials Chemistry A* 6 (47) 2018: pp. 24324 – 24329. https://doi.org/10.1039/c8ta08900k
31. **Trots, D.M., Myagkota, S.V.** High-Temperature Structural Evolution of Caesium and Rubidium Triiodoplumbates *Journal of Physics and Chemistry of Solids* 69 (10) 2008: pp. 2520 – 2526. https://doi.org/10.1016/j.jpcs.2008.05.007
32. **Tan, S., Zhang, J., Zhang, L., Gao, W., Xu, B., Zhao, Y., Wang, J., Yang, Z.** Temperature-Reliable Low-Dimensional Perovskites Passivated Black-Phase $CsPbI_3$ Toward Stable and Efficient Photovoltaics *Angewandte Chemie International Edition* 61 (23) 2022: pp. e202201300. https://doi.org/10.1002/anie.202201300
33. **Xu, P., Xu, G., Luo, Z., Fang, L.** Theoretical Study on Composition-Dependent Properties of $ZnO.nAl_2O_3$ Spinels. Part II: Mechanical and Thermophysical *Journal of the American Ceramic Society* 104 (12) 2021: pp. 6455 – 6466. https://doi.org/10.1111/jace.17997
34. **Hasan, M.M., Ali, M.S., Rahman, M.M., Sarker, M.R.** First-Principles Analysis of the Effects of Halogen Variation on the Properties of Lead-Free Novel Perovskites $AlGeX_3$ (X = F, Cl, Br, I) *ACS Omega* 9 (33) 2024: pp. 35301 – 35312. https://doi.org/10.1021/acsomega.4c00209
35. **Lang, L., Xu, B., Liu, H., Liu, W.** First-Principles Study on the Electronic and Optical Properties of Cubic ABX_3 Halide Perovskites *Physics Letters A* 378 (3) 2014: pp. 290 – 293. https://doi.org/10.1016/j.physleta.2013.11.018
36. **Arrigoni, M., Madsen, G.K.H.** Comparing the Performance of LDA and GGA Functionals in Predicting the Lattice Thermal Conductivity of III–V Semiconductor Materials in the Zincblende Structure: The Cases of AlAs and Bas *Computational Materials Science* 156 2019: pp. 354 – 360. https://doi.org/10.1016/j.commatsci.2018.10.051
37. **Rajeswarapalanichamy, R., Manikandan, V., Venkatesh, R., Prakash, K., Anbarasan, P.M.** Band Gap Engineering in Halide Cubic Perovskites $CsPbBr_3$−YIy (Y = 0, 1, 2, 3) – A DFT Study *Materials Science and Engineering: B* 258 2020: pp. 114560. https://doi.org/10.1016/j.mseb.2020.114560
38. **Moulaoui, L., Abidri, B., Ghemid, S., Slimani, R., Bouhemadou, A.** The Study of Electronic and Optical Properties of Perovskites $CH_3NH_3PbCl_3$ and $CH_3NH_3PbBr_3$ Using First Principles *E3S Web of Conferences* 229 2021: pp. 01023. https://doi.org/10.1051/e3sconf/202233600015
39. **Filip, M.R., Eperon, G.E., Snaith, H.J., Giustino, F.** Steric Engineering of Metal-Halide Perovskites with Tunable Optical Band Gaps *Nature Communications* 5 2014: pp. 5757. https://doi.org/10.1038/ncomms675
40. **Amat, A., Mosconi, E., Ronca, E., Quarti, C., Umari, P., Nazeeruddin, M.K., Grätzel, M., De Angelis, F.** Cation-Induced Band-Gap Tuning in Organohalide Perovskites: Interplay of Spin–Orbit Coupling and Octahedra Tilting *Nano Letters* 14 (6) 2014: pp. 3608 – 3616. https://doi.org/10.1021/nl5012992
41. **Afsari, M., Boochani, A., Hantezadeh, M.** Electronic, Optical and Elastic Properties of Cubic Perovskite $CsPbI_3$: Using First Principles Study *Optik* 127 (23) 2016: pp. 11433 – 11443. https://doi.org/10.1016/j.ijleo.2016.09.013
42. **Aktary, M., Kamruzzaman, M., Afrose, R.** A Comparative Study of the Mechanical Stability, Electronic, Optical and Photocatalytic Properties of $CsPbX_3$ (X = Cl, Br, I) by DFT Calculations for Optoelectronic Applications *RSC Advances* 12 (36) 2022: pp. 23704 – 23717. https://doi.org/10.1039/d2ra04591e